Fuel Processing Technology 132 (2015) 180–187

Contents lists available at ScienceDirect

Fuel Processing Technology

journal homepage: www.elsevier.com/locate/fuproc

Optimization of high surface area activated carbon production from *Enteromorpha prolifra* with low-dose activating agent

Yuan Gao, Qin-Yan Yue *, Yuan-Yuan Sun, Jia-Nan Xiao, Bao-Yu Gao, Pin Zhao, Hui Yu

Shandong Provincial Key Laboratory of Water Pollution Control and Resource Reuse, School of Environmental Science and Engineering, Shandong University, Jinan 250100, China

ARTICLE INFO

Article history:
Received 7 May 2014
Received in revised form 31 December 2014
Accepted 31 December 2014
Available online 14 January 2015

Keywords:
Dry-grind method
Response surface methodology
Low-dose activating agent
High surface area

ABSTRACT

High surface area activated carbon was prepared from *Enteromorpha prolifra* (*E. prolifra*) using few activating agents through a dry-grind strategy. The influences of pyrolysis conditions, including activating agent/char ratio, activation temperature and activation time, on specific surface area, micropore ratio and mean pore size of the obtained carbons were investigated by response surface methodology (RSM). Moreover, the relationships of micro/mesopore ratio with the surface area and mean pore size were also discussed. The optimized parameters were activating agent/char ratio of 1.1 (KOH/char), activation temperature of 850 °C and activation time of 60 min. Activated carbon prepared under optimum conditions possessed high surface area of 3038 $m^2 g^{-1}$ and large total pore volume of 2.285 $cm^3 g^{-1}$. The obtained carbon was used as an electrode material. The carbon electrode exhibited a high specific capacitance of 230 F g^{-1} at a current density of 0.5 A g^{-1} with a good capacitance retention of 86.96% at a high current density of 5.0 A g^{-1} in 6 M KOH electrolyte.

1. Introduction

Activated carbons (ACs) are extensively used in many fields, including organic pollution removal, catalyst support, energy storage, gas storage [1–6]. In recent years, the applications of ACs as electrochemical double-layer capacitor (EDLC) materials have gained a growing interest and worldwide attention [7]. According to the electrochemical double layer mechanism, the energy storage occurred at the interface of electrode material and electrolyte [8,9], hence the essential factors related to the electrochemical performance are specific surface area and pore volume. Until now, the commercial ACs with poor pore properties can hardly meet the requirement of the electrode material. Therefore, it is highly urgent to fabricate carbon materials with a high specific surface area.

It is well known that the raw precursors for the preparation of ACs are mainly exhausted non-renewable resources, such as coals, pitch, and phenol-resin [10–12]. The studies on the production of ACs from non-fossil sources are required to intensify due to more strictly environmental regulation and increasing demand in carbon materials. Until now, abundant biomass wastes such as coconut husk [13], bamboo [14], bagasse [15], lotus stalk [16], rice husk [17], corn cob [18], acacia mangium wood [19] and date stone [20] have been successfully converted into ACs. Recently, some researchers also investigated the application of *Enteromorpha prolifra* (*E. prolifra*) as a raw precursor for activated carbon synthesis [21,22]. *E. prolifra*, a green alga, is becoming more widespread in China due to the water eutrophication and the corresponding outbreak of green tides in recent years [22,23]. By June 13, 2013, the ocean area (Yellow Sea) of 6727 sq. km has been covered by *E. prolifra* based on the reports of the National Oceanic Administration. Hence, it is necessary to develop this extensively available marine biomass waste into high-value production.

In addition, another challenge is to produce ACs with high surface area using few activating agents in order to reduce the costs. The physical, chemical, and a combination of physical with chemical processes are traditional activation methods [24,25]. KOH is one of the most effective dehydrating chemical agents for the synthesis of high surface area ACs. Generally speaking, the precursor and KOH are mixed in a solution, and then the mixture is dried overnight to remove water [3,26–30]. Such processes require long operation time and waste activating agent. In this study, we adopt a dry-grind method to mix KOH with the precursor, which not only effectively eliminates the tedious dry-time but also significantly reduces the consumption of the activating agent. According to literature reviews, few researches have been performed on the optimal preparation of high surface area algae-derived ACs with low activating agent/char ratio using the RSM approach.

* Corresponding author. Tel.: +86 531 88365258; fax: +86 531 88364513.
E-mail address: qyyue58@aliyun.com (Q.-Y. Yue).

http://dx.doi.org/10.1016/j.fuproc.2014.12.048
0378-3820/

Table 1
Experimental design matrix and the response results.

Run	Coded level			Actual level of variable			Response variable		
				Ratio (x_1)	Activation temperature (°C) (x_2)	Activation time (min) (x_3)	S_{BET} ($m^2\ g^{-1}$)	V_{mic}/V_{tot} (%)	D_{AC} (nm)
1	−1	0	+1	0.5	700	90	1490.5	56.24	2.772
2	0	+1	+1	2	900	90	2482.5	8.051	3.943
3	0	+1	−1	2	900	30	2981.4	17.90	3.522
4	0	0	0	2	700	60	3060.1	51.76	2.742
5	0	0	0	2	700	60	2951.8	54.76	2.564
6	0	0	0	2	700	60	3171.5	47.47	2.821
7	−1	+1	0	0.5	900	60	2222.1	44.63	3.133
8	0	0	0	2	700	60	3068.7	50.16	2.521
9	−1	−1	0	0.5	500	60	587.49	41.52	3.572
10	+1	0	−1	3.5	700	30	2475.7	47.98	2.639
11	+1	−1	0	3.5	500	60	1017.3	61.87	2.432
12	−1	0	−1	0.5	700	30	1173.0	51.19	2.999
13	+1	+1	0	3.5	900	60	2904.4	10.53	4.670
14	0	−1	+1	2	500	90	1066.3	59.97	2.541
15	0	0	0	2	700	60	3122.2	49.61	2.771
16	+1	0	+1	3.5	700	90	2736.0	30.28	2.983
17	0	−1	−1	2	500	30	882.26	53.08	2.794

The main objectives of this work were to (i) transform *E. prolifra* wastes into ACs with high surface area using as little activating agent as possible; (ii) investigate the influences of pyrolysis parameters on the properties of the algae–carbon by RSM; and (iii) to discuss the electrochemical properties of the ACs prepared under the optimum conditions.

2. Experimental

2.1. Preparation of activated carbon

E. prolifra was procured from Shandong Province, China. *E. prolifra* was dried, crushed and sized. The obtained *E. prolifra* powder was ~0.38 mm. The proximate analysis data of *E. prolifra* are as follows: 12.94% of moisture, 60.48% of volatile matter, 19.84% of ash, 6.74% of fixed carbon and 74.99% of organic compound. The high content of organic compound indicates that *E. prolifra* has a potential as a good carbon precursor. *E. prolifera* in this study has higher ash and moisture content than those in other literatures, while the volatile matter content is lower [31,32]. These differences may derive from the various harvest time and sampling locations. The carbonization was performed without protection gas in an electric resistance furnace (KSY-4D-16) at a carbonization temperature of 500 °C and a carbonization time of 1.5 h. After carbonization, the char was cooled to room temperature. Then approximately 10 g of the char was ground to powder in company with varying amounts of KOH. Afterwards, the activation process was performed using a tubular furnace in nitrogen atmosphere. The gas flow was 300 mL min^{-1}. A self-designed ferruginous crucible was used to place the mixture and the specially-made crucible had a good anti-corrosion. After cooling, the resultant samples were washed with HCl and distilled water repeatedly to eliminate the by-product residues. The samples were dried at 110 °C for 12 h and stored in a valve bag for following studies.

2.2. Experimental design and statistical analysis

Response surface methodology (RSM) is a useful tool for building models, designing experiments, estimating effects of variables and determining optimum operating variables [33–36]. In this study, the Box–Behnken design model (BBD), a typical response surface methodology, was established to visualize the influences of independent factors or interactions among the parameters on the responses and search for the optimum operating conditions [37,38]. The BBD model consists of a total of 17 experiments, including the first 12 factorial runs and 5 repetitive runs at the central point for the evaluation of the experimental error. Three operating variables were specified: activating agent/char ratio (0.5–3.5), activation time (30 min–90 min) and activation temperature (500 °C–900 °C). The performance of the system was estimated by the analysis of the responses for the BET surface area, micropore ratio and mean pore size. The polynomial equation was employed to predict the optimal point and expressed as follows:

$$Y_i = \beta_0 + \sum \beta_i x_i + \sum \beta_{ii} x_{ii}^2 + \sum \beta_{ij} x_i x_j + e_i \quad (1)$$

where Y_i ($i = 1,2,3$) is the predicted response. X_i and x_j are the independent variables, β_0 is the constant coefficient. The parameters, β_i, β_{ii} and β_{ij} are the linear, quadratic and different interaction coefficients, respectively. The value of e_i represented the error of the model. The Design Expert 7.0 software was used for generating the statistical experimental design and analyzing the observed data [37,38]. The quality-of-fit of the model was checked by the coefficient of determination R^2 and $R_{adj}{}^2$. Furthermore, the statistical significance was determined by the analysis of variance (ANOVA) [37,38]. The model terms were evaluated according to the p-value with a confidence level of 95%. The smaller the p-value and the larger the *F*-value, the more significant is the parameter. In this study, the optimization was performed to obtain the levels of independent variables, which maximized the BET surface area and minimized the amount of KOH so as to reduce the consumption of the activating agent.

2.3. Characterization

The textural characterization of each sample was determined through nitrogen adsorption at 77 K using a JW-BK122W surface area analyzer equipped with specialized software of calculation and analysis. The BET surface area (S_{BET}) was determined based on the standard Brunauer–Emmett–Teller equation [39]. The pore size distribution of the samples was obtained according to the Barrett–Joyner–Halenda (BJH) method. The total pore volume was calculated from the amount of nitrogen adsorbed at $P/P_0 = 0.99$. The micropore volume (V_{mic}) was obtained by *t*-plot method. The mean pore size (D_{AC}) was calculated according to the Eq. (2).

$$D_{AC} = \frac{4V}{S_{BET}}. \quad (2)$$

The pyrolysis behaviors of char and char impregnated with KOH were performed by thermal gravimetric analysis (TGA) and differential

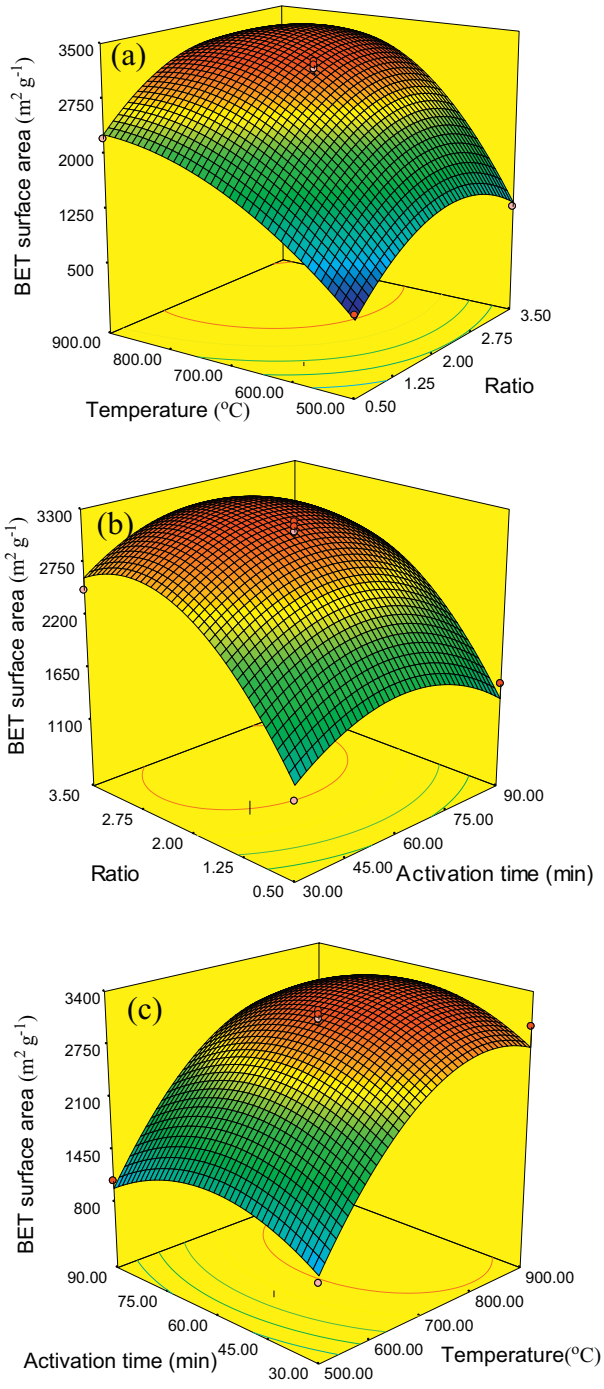

Fig. 1. The three-dimensional response surface plots (a) the effect of activation temperature and activating agent/char ratio, (b) effect of activation time and activating agent/char ratio and (c) the effect of activation time and temperature on the specific surface area.

thermal analysis (DTG), which was recorded by using a thermo analyzer (Shimadzu, TGA-50). Approximately 10 mg of the samples was placed into a crucible and heated to 800 °C in the presence of nitrogen. The heating rate was 15 °C min^{-1}, which was in accordance with that of the activation process.

2.4. Electrochemical measurements

The electrochemical performance was measured in a symmetric two-electrode experimental setup using a PARSTAT2273 electrochemical workstation. To fabricate the working electrode, the homogeneous slurry was prepared by completely mixing the carbon materials, acetylene black and polytetrafluoroethylene at a weight ratio of 85:10:5 in alcohol. The mixture was pressed onto nickel foam under the pressure of 10 Mpa and dried at 100 °C for 12 h. The mass of the activated substance loading on each electrode was about 5 ± 1 mg. Cyclic voltammetry (CV) experiment was tested in a potential window range of 0–1 V with various scan rates. The charge–discharge experiment was performed within the different current densities ranging from

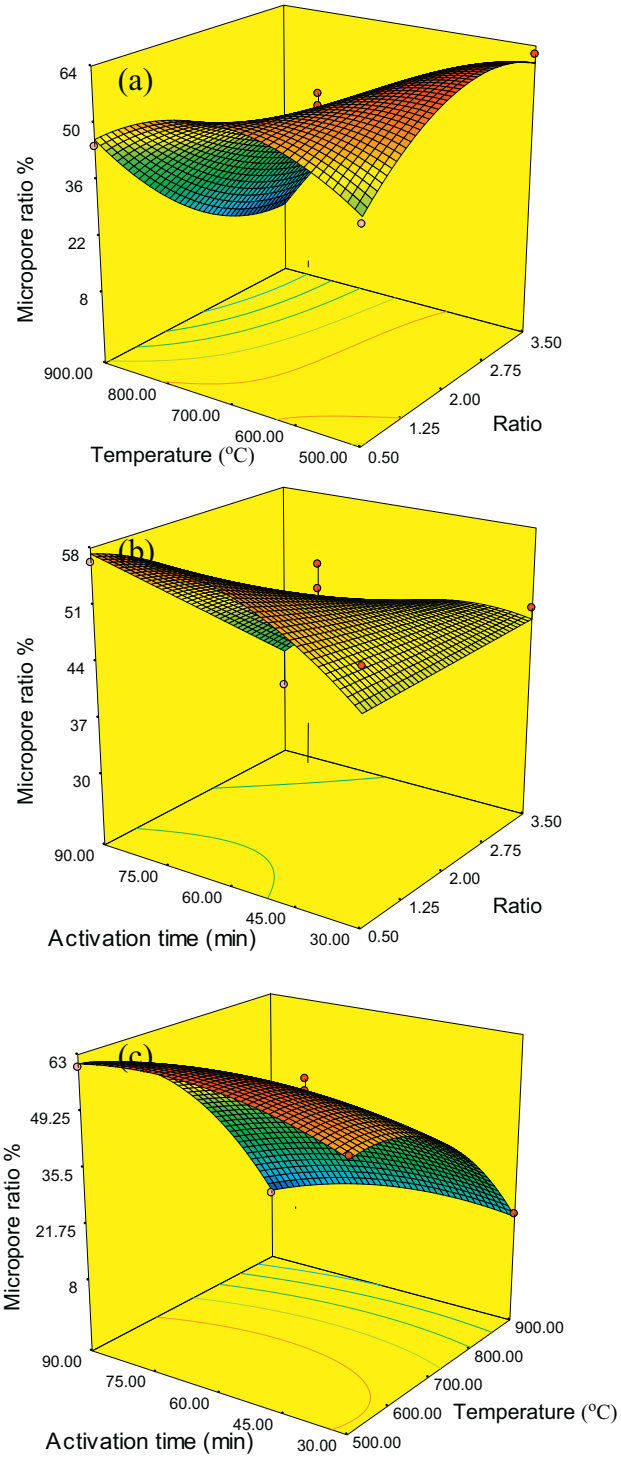

Fig. 2. The three-dimensional response surface plots (a) the effect of activation temperature and activating agent/char ratio, (b) effect of activation time and activating agent/char ratio and (c) the effect of activation time and temperature on the micropore ratio.

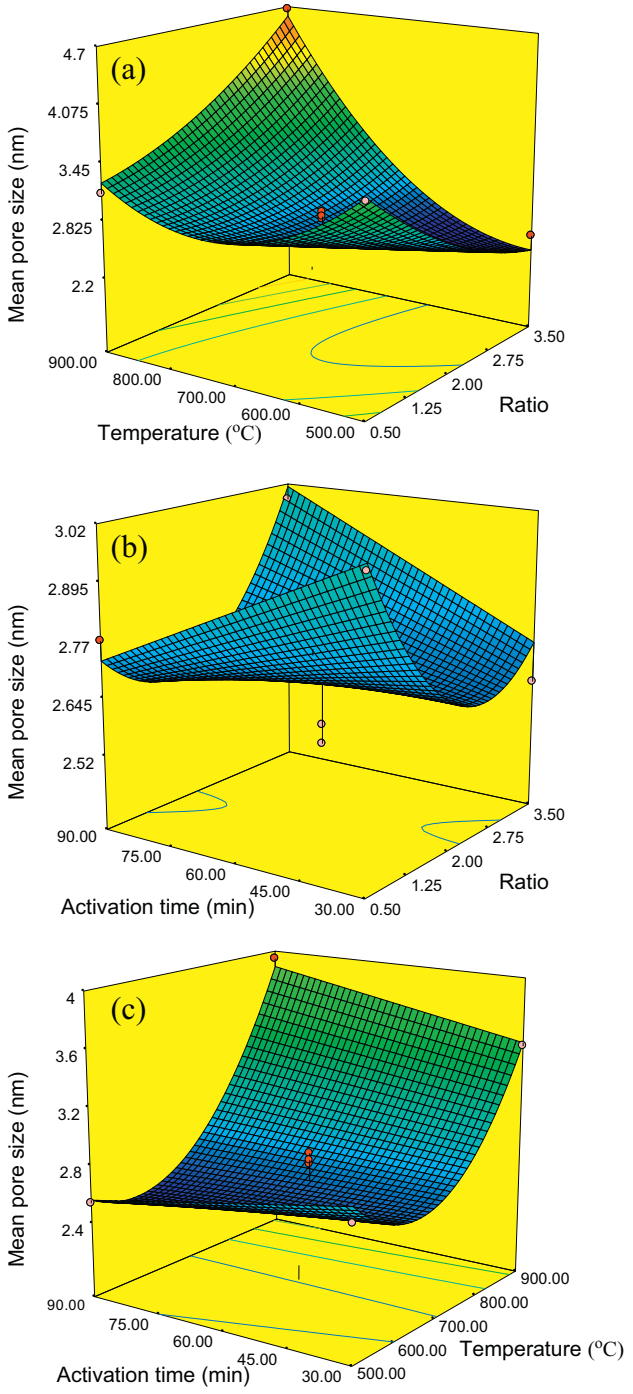

Fig. 3. The three-dimensional response surface plots (a) the effect of activation temperature and activating agent/char ratio, (b) effect of activation time and activating agent/char ratio and (c) the effect of activation time and temperature on the mean pore size.

0.5 A g^{-1} to 5 A g^{-1}. The electrochemical impedance experiment (EIS) was carried out in the frequencies ranging from 100 kHz to 100 mHz. The specific capacitances are calculated according to Eqs. (3) and Eqs. (4):

$$C_{CV} = \frac{\int Idu}{2v(2m)\Delta U} \times 4 \tag{3}$$

$$C_{CD} = \frac{I\Delta t}{2m\Delta U} \times 4 \tag{4}$$

where I is the current load (A); v is the scan rate (mV s^{-1}); m is the mass of single electrode (g); Δt is the discharge time (s); and ΔU is the potential range (V). *CCV* and *CCD* are the specific capacitances from the cyclic voltammetry experiment and the charge–discharge experiment.

3. Results and discussion

3.1. Development of regression model

The BET surface area, micropore ratio and mean pore size are the important characteristics affecting the electrochemical performance of the carbon materials. Hence, the variance analysis was performed to identify the most effective parameter and to model the relationship between the independent variables and responses. Besides, the responses were designed to investigate how to obtain the high surface area, meanwhile cutting down the consumption of the activating agent. The experimental design matrix and the corresponding response results are presented in Table 1. The refined models in terms of coded factors after excluding the insignificant terms for the specific surface area (Y_1), micropore ratio (Y_2) and mean pore size (Y_3) are given in Eqs. (5)–Eqs. (7), respectively.

$$Y_1 = 3074.86 + 457.54x_1 + 879.63x_2 - 638.18{x_1}^2 - 753.86{x_2}^2 - 467.88{x_3}^2 \tag{5}$$

$$Y_2 = 48.83 - 5.36x_1 - 16.92x_2 - 13.61x_1x_2 - 11.63{x_2}^2 \tag{6}$$

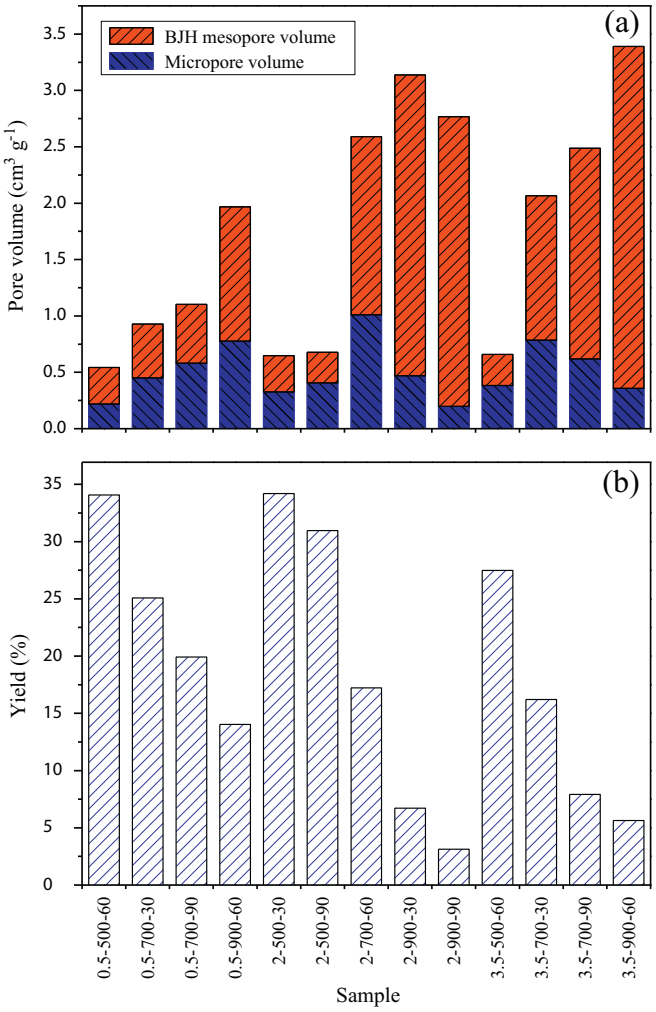

Fig. 4. Effects of preparation variables on (a) pore distribution and (b) carbon yield.

Table 2
Process optimization validation.

Ratio	Activation temperature (°C)	Activation time (min)	Predicted			Experimental		
			S_{BET}[a] ($m^2\ g^{-1}$)	V_{mic}[b] (%)	D_{AC}[c] (nm)	S_{BET}[a] ($m^2\ g^{-1}$)	V_{mic}[b] (%)	D_{AC}[c] (nm)
1.1	850	60	2806.27	38.94	3.120	3038.53	40.13	3.008

[a] BET specific surface area.
[b] Micropore volume.
[c] Mean pore size.

$$Y_3 = 2.67 + 0.49x_2 + 0.67x_1x_2 + 0.14x_1x_3 + 0.17x_2x_3 + 0.21{x_1}^2 + 0.56{x_2}^2. \quad (7)$$

The positive and negative sign in front of the terms represented the synergistic and antagonistic effects. The values of R^2 or ${R_{adj}}^2$ for three responses were almost close to 1, predicting a good agreement between the prediction and the experimental data. As Table S1 lists, the model *F*-value of 56.24 from the ANOVA for the BET surface area suggested that the model was significant. The value of Prob. > *F* was less than 0.05, indicating that the model terms were significant. As listed in Table S2, the model *F*-value of 19.86 from the ANOVA for the micropore ratio implied that the model was significant. The values of Prob. > *F* less than 0.05 illustrated that the model terms were significant. As Table S3 lists, the model *F*-value of 61.63 from the ANOVA for the mean pore size suggested that the model was also significant. Thus, the above results demonstrated that the established models could accurately predict the responses in the range of the studied variables.

3.2. Effects of preparation parameters

3.2.1. Effects of preparation variables on the specific surface area

The three-dimensional response surface plots have been recommended to be highly informative for the interpretation of the interaction behavior of the system variables. As shown in Fig. S1, the circular nature of the contours implied that the interactions between the variables were insignificant [20,40]. This result was in line with the three dimensional plots (Fig. 1) and the variance analysis data (Table S1). The activation temperature had the most prominent contribution to the specific surface area according to the highest *F*-value of 129.35. The activating agent/char ratio had the secondary influence. And the influence of activation time was negligible. Therefore, the activation temperature should be intensively taken into consideration for the preparation of the activated carbon with high surface area. As demonstrated in Fig. S2, the BET surface area was found to ascend from 1441 $m^2\ g^{-1}$ to the peak and then glide down to 3200 $m^2\ g^{-1}$ with the rise of temperature from 500 to 900 °C. A similar trend was also observed in the case of the activating agent/char ratio. In particular, the activation time plot appeared to be an almost symmetrical parabolic shape. As the time rose, the BET surface area increased up to the maxima. Afterwards, further rise in activation time led to the decrease of the specific surface area. Because the suitable increased variables produced a positive effect on the generation of new pores in carbon framework, contributing to the high surface area. However, an excess increase will lead to the collapse of the pore structure due to a more intensified dehydration [41].

3.2.2. Effects of preparation variables on micropore ratio

The micropore ratio is an essential factor not only related to the specific surface area but also involved in the electrochemical performance. As illustrated in Fig. 2(a–c), the effects of the operating factors on the micropore ratio are examined by three-dimensional response surface plots. The interaction of the activating agent/char ratio and temperature possessed a huge impact on the micropore ratio with a high *F*-value of 15.36 (Table S2). It was evident that the effects of the single factor on the micropore ratio were in the order: activation temperature ≫ activating agent/char ratio > activation time. Interestingly, the effects of the single operating factor on the micropore ratio were performed in totally three different situations. Fig. S3 reveals that the micropore ratio linearly gradually decreased from 56.23% to 45.50% with the increasing activating agent/char ratio. A drastic decreasing trend from 61.27% to 17.72% was observed with the increase of the activation temperature. Nevertheless, the micropore ratio was found to increase gradually to a peak and then decrease with an increasing activation time. The intensification of the dehydration reaction was caused by the increase of operating parameters, which contributed to the transformation of the micropores to the meso/macropores.

3.2.3. Effects of preparation variables on mean pore size

A small pore size may increase the resistance of the electrolyte ion into the pores, further resulting in a dramatic degradation of the overall performance of the supercapacitors. So the effects of experimental variables on the mean pore size of the carbon material are necessary. As shown in Table S3 and Fig. 3(a–c), the interaction of the activation temperature and the activating agent/char ratio was found to be more important than the other combinations. The three-dimensional response surface plots show that the most important variable for the mean pore size was the activation temperature. The activating agent/char ratio and the activation time have slight effects on the mean pore size. The mean pore size gradually decreased to 2.564 nm and then increased to 3.71 nm with the increase of the activation temperature (Fig. S4). This phenomenon can be explained by analyzing the transformation between the micropores and the mesopores. Fig. 4(a) reveals that the micropore volume firstly increased and then decreased during the whole

Table 3
Comparison of the pore structures of prepared activated carbon by KOH activation.

Precursor	Activating agent ratio	S_{BET}[a] ($m^2\ g^{-1}$)	V_{tot}[b] ($cm^3\ g^{-1}$)	V_{mic}[c] ($cm^3\ g^{-1}$) (%)	Reference
E. prolifra	1.1:1	3038	2.285	0.917	This work
Siris seed pods	1:1	1824	0.782	0.645	[26]
Waste biomass	1:1	618	0.291	0.143	[27]
Spartina alterniflora	1:1	1161	0.553	0.532	[28]
Cane pith	2:1	912	0.53	0.418	[29]
Coal residue	2:1	1634	1.00	0.140	[30]
Corncob	4:1	3012	1.70	0.98	[3]

[a] BET specific surface area.
[b] Total pore volume.
[c] Micropore volume.

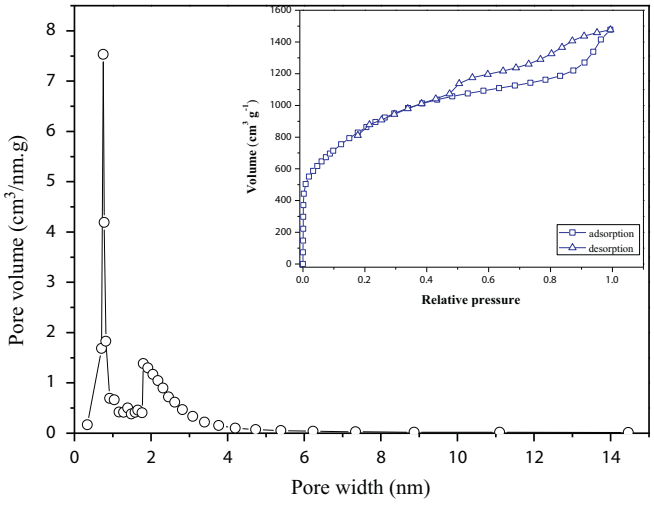

Fig. 5. Pore size distribution and nitrogen adsorption isotherm (inset) of the activated carbon under the optimum condition.

temperature at the activating agent/char ratio of 2 and 3.5, while the mesopore volume increased all the time. Herein, the growth of the micropore may lead to the reduction of the mean pore size and the increase of the mesopore may enlarge the mean pore size. Meanwhile, these results can be also used to explain the relationship between the micro/mesopores and the surface area. As we all know, the microspores are the main contributors to the high surface area of ACs. On the contrary, more meso/macropores will reduce the surface area of ACs. As shown in Fig. 4(b), three parameters all have a negative effect on the carbon yields.

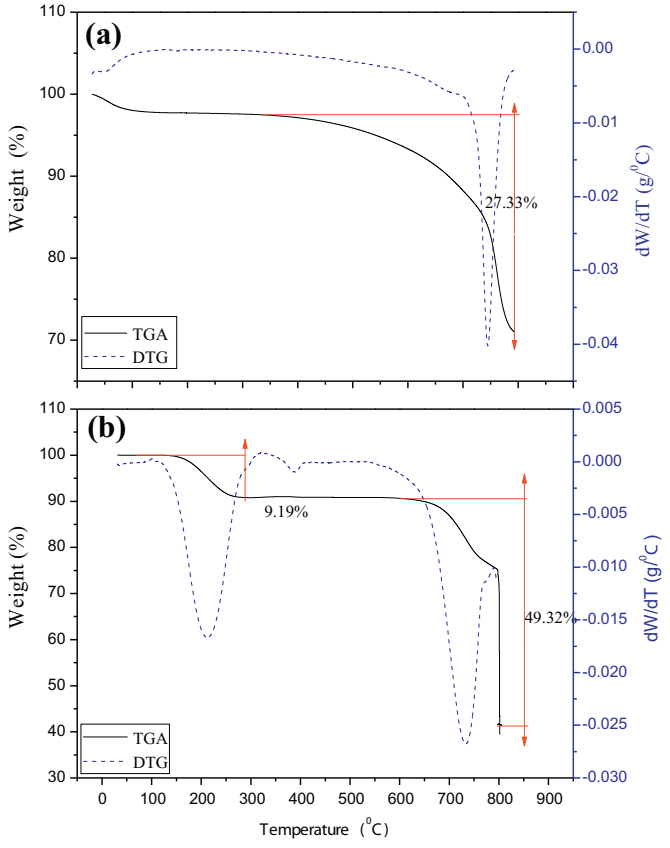

Fig. 6. TGA and DTG curves for (a) char and (b) char impregnated with KOH at a ratio of 1.1.

3.3. Process optimization

One of the main objectives of this study was to obtain the optimum process parameters in which the carbon can be produced with high surface area using as little activating agent as possible for economical feasibility. In order to compromise the three different responses, the function of desirability was introduced with Design Expert software 7.0. The optimum preparation conditions are given in Table 2, accompanied with the experimental and predicted values. For simplicity and practical application, the optimum carbon was obtained by using: activating agent/char ratio of 1.1, activation temperature of 850 °C and activation time of 60 min. It was observed that there were small errors between the experimental and predicted values, which were 7.64%, 2.97% and 3.72% for the specific surface area, the micropore ratio and the mean pore size. Activated carbon prepared under optimum conditions has a high surface area of 3038 $m^2\ g^{-1}$ and a large total pore volume of 2.285 $cm^3\ g^{-1}$.

3.4. Characterization of ACs prepared under optimum conditions

3.4.1. Porous structure analysis

As listed in Table 3, the porous properties of carbon prepared in this study are superior to carbons derived from other raw precursors at different activating agent/char ratios using the conventional solution-mixing method. It can be ascertained that the carbon with a BET specific surface area in excess of 3000 $m^2\ g^{-1}$ could be produced with a much lower activating agent/char ratio than those of other studies. In other words, the solid-grind is an extraordinary useful approach to produce carbons with high surface area. As Fig. 5 exhibits, the isotherm of the activated carbon prepared under the optimum exhibited a combination of type I and type IV with an obvious H3 hysteresis loop, implying the presence of slit-like pores [42,43]. This type of isotherm demonstrated the coexistence of the micropores, mesopores and macropores. The micropore volume contributed approximately about 40.13% to the total pore volume. Such hierarchical structure is beneficial to the excellent electrochemical performances [44,45].

3.4.2. Thermal behavior analysis

The thermal stability of the raw material was characterized by TGA–DTG. It is evident that remarkable differences were observed in the intensity, number and location of peaks in the DTG profiles (Fig. 6(a)). A remarkable modification in pyrolysis was caused by the addition of the activating agent, KOH. The DTG curves in Fig. 6(b) demonstrated that a fresh peak appeared around 380 °C compared to the pure char pyrolysis. This peak was assigned to a chemical reaction by the fusion of KOH.

Furthermore, the char showed one step to weight loss, yet the char–KOH sample displayed three steps. In Fig. 6(a), before the 400 °C temperature, no obvious weight loss was observed. At the 800 °C temperature, the recorded mass loss was 27.33%. In Fig. 6(b), only 9.19% of mass loss was observed between the temperatures of 31 °C and 290 °C, reflected as a broad peak around the temperature of 210 °C in the DTG curve. It was likely attributed to the moisture and low molecular weight volatile constituents. In the temperature range of 290 °C to 600 °C, the thermal degradation proceeded very slowly. Between the temperatures of 600 °C and 797 °C, the mass loss was 15.65%. Moreover, the maximum mass loss of 33.67% was recorded during the constant temperature course, which was attributable to the evaporation of carbon dioxide, carbon monoxide, elementary potassium and other pyrolysis products [46]. The difference between the total weight losses of the two samples reflected the powerful dehydration and condensation roles using potassium hydroxide as the activating agent.

3.4.3. Electrochemical performance analysis

Cyclic voltammetry test can provide the significant information on the electrochemical behavior directly. Obviously, the cyclic voltammogram

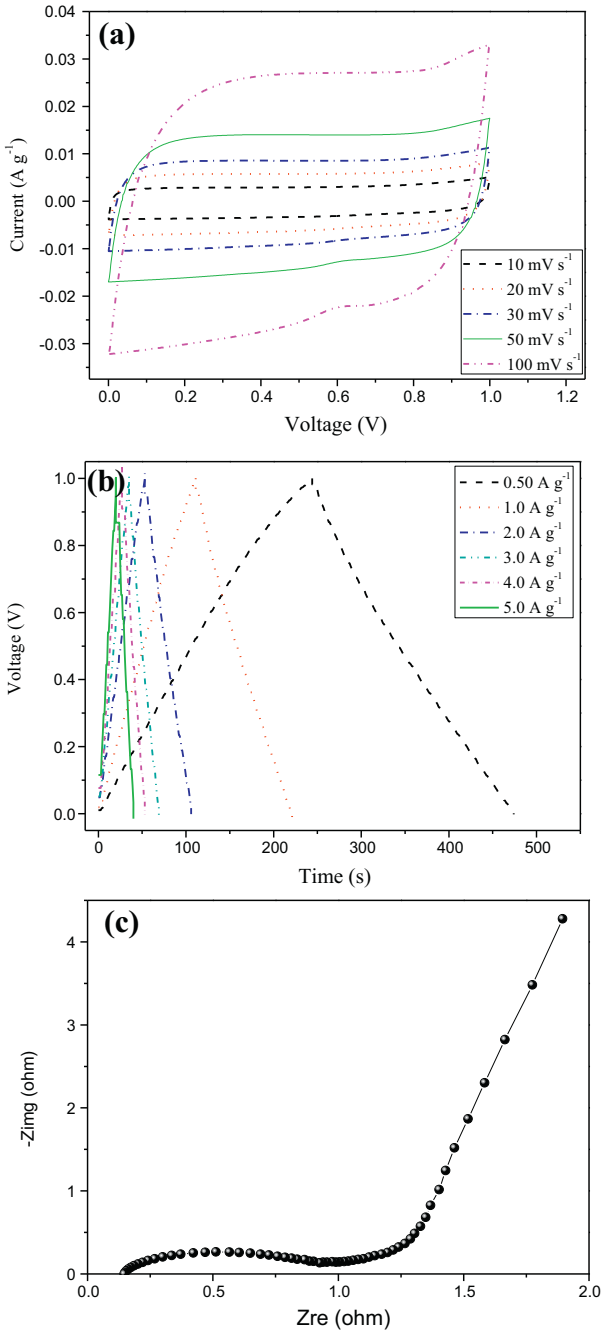

Fig. 7. (a) Cyclic voltammograms at different scan rates, (b) galvanostatic charge–discharge curves at different current densities and (c) Nyquist plots for the carbon prepared under optimum conditions.

curve still presents a relatively rectangular shape without any redox peaks even at a high scan rate, indicating a good charge propagation capability (Fig. 7(a)). The obtained carbon showed a high capacitance of 214 F g^{-1} at a scan rate of 10 mV s^{-1} and the specific capacitance retained 74.29% even at a high scan rate of 100 mV s^{-1}, which may be due to the high surface area of the prepared carbon. As shown in Fig. 7(b), all galvanostatic charge–discharge curves display regularly triangular shapes, suggesting the good capacitive properties of the carbon electrodes. The specific capacitance is 230 F g^{-1} at a current density of 0.5 A g^{-1}, and the specific capacitance is still relative high (200 F g^{-1}) at a higher current density of 5.0 A g^{-1} with a retention of 86.96%. The electrochemical impedance measurement was conducted to obtain complementary information about the electrochemical frequency behavior of the system. The Nyquist plot is showed in Fig. 7(c) and the data of the Nyquist plots was fitted using the ZSimpWin software. The equivalent series resistance is 0.1765 Ω for the electrode, implying a high charging–discharging rate of the electrode material. What's more, a vertical nature of the plot at low frequency means a near-ideal electric double layer capacitor behavior for the electrode [8].

4. Conclusions

The high surface area activated carbons were produced using as little activating agent as possible through a dry-grind approach. The optimum conditions according to the Box–Behnken design were found to be the activating agent/char ratio of 1.1, activation temperature of 850 °C and activation time of 60 min. Besides, the activation temperature has the greatest influence on the properties of the carbons. The TGA–DTG curves showed the powerful dehydration and condensation roles using potassium hydroxide as the activating agent. Furthermore, the activated carbon possessed excellent electrochemical property as an electrode material for the supercapacitor. The results indicated that the synthesis of the activated carbon from *E. prolifera* is a promising way for the high value conversion of this marine waste.

Acknowledgments

This work was financially supported by the National Science Fund for Distinguished Young Scholar (21307075). The authors thank 3 anonymous reviewers and editor for their good suggestions, which substantially improved the manuscript.

Appendix A. Supplementary data

Supplementary data to this article can be found online at http://dx.doi.org/10.1016/j.fuproc.2014.12.048.

References

[1] A.L. Cazetta, A.M.M. Vargas, E.M. Nogami, M.H. Kunita, M.R. Guilherme, A.C. Martins, T.L. Silva, J.C.G. Moraes, V.C. Almeida, NaOH-activated carbon of high surface area produced from coconut shell: kinetics and equilibrium studies from the methylene blue adsorption, Chemical Engineering Journal 174 (2011) 117–125.
[2] S.-H. Du, L.-Q. Wang, X.-T. Fu, M.-M. Chen, C.-Y. Wang, Hierarchical porous carbon microspheres derived from porous starch for use in high-rate electrochemical double-layer capacitors, Bioresource Technology 139 (2013) 406–409.
[3] Y. Sun, P.A. Webley, Preparation of activated carbons from corncob with large specific surface area by a variety of chemical activators and their application in gas storage, Chemical Engineering Journal 162 (2010) 883–892.
[4] D. Xin-hui, C. Srinivasakannan, P. Jin-hui, Z. Li-bo, Z. Zheng-yong, Preparation of activated carbon from Jatropha hull with microwave heating: optimization using response surface methodology, Fuel Processing Technology 92 (2011) 394–400.
[5] B. Tsyntsarski, S. Marinov, T. Budinova, M.F. Yardim, N. Petrov, Synthesis and characterization of activated carbon from natural asphaltites, Fuel Processing Technology 116 (2013) 346–349.
[6] N.G. Asenjo, C. Botas, C. Blanco, R. Santamaría, M. Granda, R. Menéndez, P. Alvarez, Synthesis of activated carbons by chemical activation of new anthracene oil-based pitches and their optimization by response surface methodology, Fuel Processing Technology 92 (2011) 1987–1992.
[7] X. Li, W. Xing, S. Zhuo, J. Zhou, F. Li, S.Z. Qiao, G.Q. Lu, Preparation of capacitor's electrode from sunflower seed shell, Bioresource Technology 102 (2011) 1118–1123.
[8] J. Zhang, L. Jin, J. Cheng, H. Hu, Hierarchical porous carbons prepared from direct coal liquefaction residue and coal for supercapacitor electrodes, Carbon 55 (2013) 221–232.
[9] K. Xia, Q. Gao, J. Jiang, J. Hu, Hierarchical porous carbons with controlled micropores and mesopores for supercapacitor electrode materials, Carbon 46 (2008) 1718–1726.
[10] Y. Zhu, X. Xiang, E. Liu, Y. Wu, H. Xie, Z. Wu, Y. Tian, An activated microporous carbon prepared from phenol–melamine–formaldehyde resin for lithium ion battery anode, Materials Research Bulletin 47 (2012) 2045–2050.
[11] C. Zeng, Q. Lin, C. Fang, D. Xu, Z. Ma, Preparation and characterization of high surface area activated carbons from co-pyrolysis product of coal-tar pitch and rosin, Journal of Analytical and Applied Pyrolysis 104 (2013) 372–377.
[12] G.-z. Gong, Q. Xie, Y.-f. Zheng, S.-F. Ye, Y.-F. Chen, Regulation of pore size distribution in coal-based activated carbon, New Carbon Materials 24 (2009) 141–146.
[13] I.A. Tan, A.L. Ahmad, B.H. Hameed, Adsorption of basic dye on high-surface-area activated carbon prepared from coconut husk: equilibrium, kinetic and thermodynamic studies, Journal of Hazardous Materials 154 (2008) 337–346.

[14] G.-Q. Wu, X. Zhang, H. Hui, J. Yan, Q.-S. Zhang, J.-L. Wan, Y. Dai, Adsorptive removal of aniline from aqueous solution by oxygen plasma irradiated bamboo based activated carbon, Chemical Engineering Journal 185–186 (2012) 201–210.
[15] K.Y. Foo, L.K. Lee, B.H. Hameed, Preparation of activated carbon from sugarcane bagasse by microwave assisted activation for the remediation of semi-aerobic landfill leachate, Bioresource Technology 134 (2013) 166–172.
[16] H. Liu, J. Zhang, C. Zhang, N. Bao, C. Cheng, Activated carbons with well-developed microporosity and high surface acidity prepared from lotus stalks by organophosphorus compounds activations, Carbon 60 (2013) 289–291.
[17] R. Farma, M. Deraman, A. Awitdrus, I.A. Talib, E. Taer, N.H. Basri, J.G. Manjunatha, M.M. Ishak, B.N.M. Dollah, S.A. Hashmi, Preparation of highly porous binderless activated carbon electrodes from fibres of oil palm empty fruit bunches for application in supercapacitors, Bioresource Technology 132 (2013) 254–261.
[18] S. Nethaji, A. Sivasamy, A.B. Mandal, Preparation and characterization of corn cob activated carbon coated with nano-sized magnetite particles for the removal of Cr(VI), Bioresource Technology 134 (2013) 94–100.
[19] M. Danish, R. Hashim, M.N.M. Ibrahim, O. Sulaiman, Effect of acidic activating agents on surface area and surface functional groups of activated carbons produced from *Acacia mangium* wood, Journal of Analytical and Applied Pyrolysis 104 (2013) 418–425.
[20] M. Danish, R. Hashim, M.N.M. Ibrahim, O. Sulaiman, Optimized preparation for large surface area activated carbon from date (*Phoenix dactylifera* L.) stone biomass, Biomass and Bioenergy 61 (2014) 167–178.
[21] M. Wang, F. Hao, G. Li, J. Huang, N. Bao, L. Huang, Preparation of *Enteromorpha prolifera*-based cetyl trimethyl ammonium bromide-doped activated carbon and its application for nickel(II) removal, Ecotoxicology and Environmental Safety 104 (2014) 254–262.
[22] Y. Li, Q. Du, X. Wang, P. Zhang, D. Wang, Z. Wang, Y. Xia, Removal of lead from aqueous solution by activated carbon prepared from *Enteromorpha prolifera* by zinc chloride activation, Journal of Hazardous Materials 183 (2010) 583–589.
[23] A. Özer, G. Gürbüz, A. Çalimli, B.K. Körbahti, Biosorption of copper(II) ions on *Enteromorpha prolifera*: Application of response surface methodology (RSM), Chemical Engineering Journal 146 (2009) 377–387.
[24] M. Hejazifar, S. Azizian, H. Sarikhani, Q. Li, D. Zhao, Microwave assisted preparation of efficient activated carbon from grapevine rhytidome for the removal of methyl violet from aqueous solution, Journal of Analytical and Applied Pyrolysis 92 (2011) 258–266.
[25] Y.-B. Tang, Q. Liu, F.-Y. Chen, Preparation and characterization of activated carbon from waste ramulus mori, Chemical Engineering Journal 203 (2012) 19–24.
[26] M.J. Ahmed, S.K. Theydan, Microporous activated carbon from *Siris* seed pods by microwave-induced KOH activation for metronidazole adsorption, Journal of Analytical and Applied Pyrolysis 99 (2013) 101–109.
[27] T. Tay, S. Ucar, S. Karagoz, Preparation and characterization of activated carbon from waste biomass, Journal of Hazardous Materials 165 (2009) 481–485.
[28] J. Liu, Y. Li, K. Li, Optimization of preparation of microporous activated carbon with high surface area from *Spartina alterniflora* and its *p*-nitroaniline adsorption characteristics, Journal of Environmental Chemical Engineering 1 (2013) 389–397.
[29] R.L. Tseng, S.K. Tseng, Characterization and use of high surface area activated carbons prepared from cane pith for liquid-phase adsorption, Journal of Hazardous Materials 136 (2006) 671–680.
[30] J. Zhang, L. Jin, S. Liu, Y. Xun, H. Hu, Mesoporous carbon prepared from direct coal liquefaction residue for methane decomposition, Carbon 50 (2012) 952–959.
[31] D. Li, L. Chen, J. Zhao, X. Zhang, Q. Wang, H. Wang, N. Ye, Evaluation of the pyrolytic and kinetic characteristics of *Enteromorpha prolifera* as a source of renewable biofuel from the Yellow Sea of China, Chemical Engineering Research and Design 88 (2010) 647–652.
[32] W. Yang, X. Li, S. Liu, L. Feng, Direct hydrothermal liquefaction of undried macroalgae *Enteromorpha prolifera* using acid catalysts, Energy Conversion and Management 87 (2014) 938–945.
[33] R. Hoseinzadeh Hesas, A. Arami-Niya, W.M.A. Wan Daud, J.N. Sahu, Preparation of granular activated carbon from oil palm shell by microwave-induced chemical activation: optimisation using surface response methodology, Chemical Engineering Research and Design 91 (2013) 2447–2456.
[34] F. Karacan, U. Ozden, S. Karacan, Optimization of manufacturing conditions for activated carbon from Turkish lignite by chemical activation using response surface methodology, Applied Thermal Engineering 27 (2007) 1212–1218.
[35] M.A. Bezerra, R.E. Santelli, E.P. Oliveira, L.S. Villar, L.A. Escaleira, Response surface methodology (RSM) as a tool for optimization in analytical chemistry, Talanta 76 (2008) 965–977.
[36] V. Silva, A. Rouboa, Optimizing the gasification operating conditions of forest residues by coupling a two-stage equilibrium model with a response surface methodology, Fuel Processing Technology 122 (2014) 163–169.
[37] M. Heydari Majd, A. Rajaei, D. Salar Bashi, S.A. Mortazavi, S. Bolourian, Optimization of ultrasonic-assisted extraction of phenolic compounds from bovine pennyroyal (*Phlomidoschema parviflorum*) leaves using response surface methodology, Industrial Crops and Products 57 (2014) 195–202.
[38] P. Balasubramani, R. Viswanathan, M. Vairamani, Response surface optimisation of process variables for microencapsulation of garlic (*Allium sativum* L.) oleoresin by spray drying, Biosystems Engineering 114 (2013) 205–213.
[39] E.P. Barrett, L.G. Joyner, P.P. Halenda, The determination of pore volume and area distributions in porous substances. I. Computations from nitrogen isotherms, Journal of the American Chemical Society 73 (1951) 373–380.
[40] K. Anupam, S. Dutta, C. Bhattacharjee, S. Datta, Adsorptive removal of chromium(VI) from aqueous solution over powdered activated carbon: optimisation through response surface methodology, Chemical Engineering Journal 173 (2011) 135–143.
[41] C. Saka, BET, TG–DTG, FT-IR, SEM, iodine number analysis and preparation of activated carbon from acorn shell by chemical activation with $ZnCl_2$, Journal of Analytical and Applied Pyrolysis 95 (2012) 21–24.
[42] Q. Wang, J. Yan, Y. Wang, T. Wei, M. Zhang, X. Jing, Z. Fan, Three-dimensional flower-like and hierarchical porous carbon materials as high-rate performance electrodes for supercapacitors, Carbon 67 (2014) 119–127.
[43] D. Angın, E. Altintig, T.E. Köse, Influence of process parameters on the surface and chemical properties of activated carbon obtained from biochar by chemical activation, Bioresource Technology 148 (2013) 542–549.
[44] Z. Zheng, Q. Gao, Hierarchical porous carbons prepared by an easy one-step carbonization and activation of phenol–formaldehyde resins with high performance for supercapacitors, Journal of Power Sources 196 (2011) 1615–1619.
[45] R.-W. Fu, Z.-H. Li, Y.-R. Liang, F. Li, F. Xu, D.-C. Wu, Hierarchical porous carbons: design, preparation, and performance in energy storage, New Carbon Materials 26 (2011) 171–179.
[46] A.-N.A. El-Hendawy, An insight into the KOH activation mechanism through the production of microporous activated carbon for the removal of Pb^{2+} cations, Applied Surface Science 255 (2009) 3723–3730.